Configurational thermodynamics of the Fe-Cr σ phase

Evgeniya Kabliman, Peter Blaha, and Karlheinz Schwarz
Institute of Materials Chemistry, Vienna University of Technology, Getreidemarkt 9/165-TC, A-1060 Vienna, Austria

Oleg E. Peil
I. Institut of Theoretical Physics, Hamburg University, Jungiusstrasse 9, D-20355 Hamburg, Germany

Andrei V. Ruban and Börje Johansson
Department of Materials Science and Engineering, Applied Material Physics, Royal Institute of Technology, Brinellvägen 23, SE-100 44 Stockholm, Sweden

(Received 29 August 2011; revised manuscript received 2 November 2011; published 17 November 2011)

Configurational thermodynamics of the Fe-Cr sigma phase is investigated on the basis of an Ising-type configurational Hamiltonian and a single-site mean-field model for the free energy. The parameters of the statistical models are obtained from efficient first-principles calculations using different computational techniques. We demonstrate that the effective pair and multisite interactions in the σ phase are relatively small, which allows using a simplified model for distributing Fe and Cr atoms among sublattices. We also show that this system exhibits a nontrivial magnetic behavior at high temperatures, which affects the site occupation by Fe and Cr atoms. The structural variation (volume and c/a) that might be present due to neutron irradiation and thermal expansion can lead to an additional atomic redistribution.

DOI: 10.1103/PhysRevB.84.184206 PACS number(s): 71.15.Mb, 71.15.Nc, 71.23.−k, 75.50.Bb

I. INTRODUCTION

Alloys based on the Fe-Cr system are of great importance for materials science due to their potential applications in the nuclear industry, which still provides an important energy source. One of the main problems of this alloy is an accurate description of its phase stability and in particular, the stability of the so-called σ phase. The σ phase produces a large impact on the alloy structure and its mechanical and thermodynamic properties: when it precipitates it has a destructive effect on the mechanical properties of the alloy. It decreases both the ductility and corrosion resistance of the material, but it also promotes the formation of cracks leading to high temperature failure, metal dusting, and loss of toughness during heat treatment and welding.[1]

The Fe-Cr σ phase is formed in a quite narrow concentration ($0.462 < x_{Cr} < 0.505$) and temperature range (700 K $< T <$ 1100 K).[2–4] Although it is paramagnetic at ambient temperatures, it becomes ferromagnetic at low temperatures (below 50 K) with a small magnetic moment.[5–8] It has a topologically closed packed structure which is defined by a tetragonal unit cell (space group $P4_2/mnm$) containing 30 atoms divided into five nonequivalent groups of sites or sublattices (A,B,C,D,E).[2,9] The crystal structure of the σ phase can be described as a stacking of the kagome tiles with the $A(0,0,0)$, $B(x,x,0)$, $C(x,y,0)$, and $D(x,y,0)$ atoms lying in the tile plane and the $E(x,x,z)$ atoms placed between the pseudohexagonal rings of the kagome tile[9] (see Fig. 1). The general formula of the σ phase can be defined as $A_2^{12}B_4^{15}C_8^{14}D_8^{12}E_8^{14}$, where the bottom and top indices denote the site multiplicities and coordination numbers for each sublattice, respectively.

The alloy components partially occupy all the nonequivalent sites but exhibit certain site preferences. In 1955 Kasper and Waterstrat performed a neutron and x-ray diffraction study in Fe-V, Ni-V, and Mn-Cr alloys and suggested a general scheme for the ordering of binary σ phases of first-row transition metal elements (and those containing Mo).[10] It was found that the highly coordinated B sites are predominately occupied by the elements to the left of Mn in the periodic table (V, Cr, Mo), the A and D sublattice with icosahedral environment are almost exclusively occupied by elements to the right of manganese (Fe, Co, Ni), whereas the C and E sites are partially occupied by both components with proportions depending on the specific alloy and external conditions.

The distribution of Fe and Cr on the sublattices in the σ phase has been investigated using *ab initio* methods in a number of recent publications.[11–16] In particular, a Connolly-Williams approach[17] has been used in Ref. 11 to represent the configurational dependent part of the total energy of the σ phase within an Ising configurational Hamiltonian. A similar scheme, but in the so-called compound energy formalism, has been used by Korzhavyi *et al.*[13] In general, the Ising-type Hamiltonian representation of the total energy is a commonly used method to solve the statistical thermodynamics problem. However, as discussed below, this formalism can become cumbersome in the case of such complicated systems as the σ phase.

In fact, until now only its simplified version has been used, without any distinction between sites of a specific sublattice. In this case the effective cluster interactions (ECIs) of the corresponding configurational Hamiltonian are obtained by fitting total energies of the σ phase with the five sublattices (A,B,C,D,E) occupied exclusively either by Cr or Fe atoms. There are $2^5 = 32$ ordered atomic arrangements for a single unit cell in the whole concentration range which can be used to extract the same number of interaction parameters. In fact this approach has even been used for ternary σ phases like Cr-Ni-Re, where $3^5 = 243$ ordered configurations were calculated in order to extract the ECIs for the whole concentration range.[18] However, these interaction parameters cannot be used for the investigation of ordering effects on the same sublattice and besides, they are likely to produce a less accurate cluster

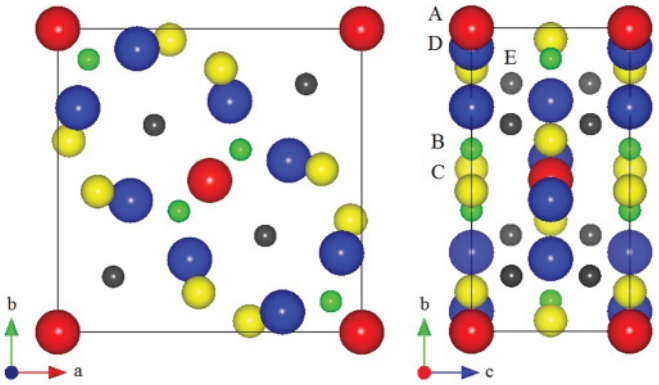

FIG. 1. (Color online) The tetragonal unit cell of the Fe-Cr σ-phase structure with five crystallographically inequivalent sites (*A*,*B*,*C*,*D*,*E*).

expansion for the range of the relevant compositions because of its restricted number of configurations and the inclusion of completely irrelevant configurations (for instance, outside the actual concentration range of the existing σ phase).

Alternatively, we recently proposed a simple approach to calculate the atomic site occupancies in binary σ phases.[19,20] With a simple single-site mean-field model, we can take into account the relevant experimental conditions and parameters of the systems and thus produce results which are in very good agreement with the available experimental data. In the present paper we investigate the reason behind its success. In particular, we show its connection to a general Ising-type model for the σ phase, whose parameters we estimate using direct *ab initio* calculations and some simple arguments. We also study how the atomic site distribution in the Fe-Cr σ phase depends on different factors such as different magnetic states, temperature effects, or structural variations which might be present due to possible thermal expansion or neutron irradiation.

II. CONFIGURATIONAL HAMILTONIAN AND EFFECTIVE CLUSTER INTERACTIONS

A. Geometrical structure

The configurational Hamiltonian of the σ phase can be written in the usual Ising form for an inhomogeneous binary alloy with five different sublattices as

$$H_{\rm conf} = E_0 + \sum_{\alpha=1,5}\sum_{i} V_{\alpha}^{(1)}\delta c_{\alpha;i} + \frac{1}{2}\sum_{\alpha,\beta=1,5}\sum_{p}\sum_{i,j\in p} V_{\alpha\beta,p}^{(2)}\delta c_{\alpha;i}\delta c_{\beta;j} + \frac{1}{3}\sum_{\alpha,\beta,\gamma=1,5}\sum_{t}\sum_{i,j,k\in t} V_{\alpha\beta\gamma,t}^{(3)}\delta c_{\alpha;i}\delta c_{\beta;j}\delta c_{\gamma;k} + \ldots, \quad (1)$$

where $V_{\alpha}^{(1)}$, $V_{\alpha\beta,p}^{(2)}$, and $V_{\alpha\beta\gamma,t}^{(3)}$ are on-site, pair, and three-site effective cluster interactions for specific sublattices (α, β, and γ) and coordination shells identified here by p for pair effective interactions and t for the three-site interactions; $\delta c_{\alpha,i}$ is the concentration fluctuation: $\delta c_{\alpha,i} = c_{\alpha,i} - c_{\alpha}$, where $c_{\alpha,i} = 1$ if Cr occupies site i of sublattice α, otherwise it is equal to 0 and $c_{\alpha} \equiv \langle c_{\alpha,i}\rangle$ is the concentration of Cr on sublattice α. Let us note that in this context "sites" refers to all lattice sites in the system but should not be confused with the term "sites" that is used in a simplified mean-field expression for the free energy of the σ phase, defined for its *unit* cell.

The ECIs in (1) depend on the whole set of concentrations on sublattices $\{c_{\alpha}\}$. The on-site effective interactions $V_{\alpha}^{(1)}$ are the zero-temperature effective chemical potentials of the corresponding sublattices. Pair effective interactions $V_{\alpha\beta,p}^{(2)}$ as well as multisite interactions are defined for the corresponding geometrically distinct sets of sites of the σ-phase structure, such as *coordination shells* for atomic pairs for the two-site interactions, triangles for the three-site interactions, and so on. The term coordination shell refers to a set of neighbor atoms (shell) located at a given distance around a chosen atom. In the high-symmetry structures, for instance, in the bcc structure, an atom is surrounded by the first nearest-neighbor shell, which forms a cube and contains eight atoms that all have the same distance; the next shell contains six atoms, and so on. In case of a low-symmetry structure, as the σ phase is, such coordination shells are, however, distorted and one usually speaks about *coordination polyhedra*, which are formed around each atom. For illustration purposes we have chosen one of the σ-phase sublattices, namely, the *E* sublattice, as shown in the inset of Fig. 2. An *E* atom is surrounded by a coordination polyhedron which consists of 14 atoms of various types. The distances of these atoms to the central one are given in the lowest section of Table I and vary from 1.60 to 2.07 (in the units of the Wigner-Seitz radius). This coordination polyhedron consists of nine coordination shells, each of which contain only one or two atoms, in contrast to the high-symmetry case of the bcc lattice. The total number of atoms which form a polyhedron around a nonequivalent atom in the σ-phase cell is referred to as a "coordination number" in the general formula $A_2^{12}B_4^{15}C_8^{14}D_8^{12}E_8^{14}$ mentioned above but is distinct from the usual term "coordination (shell) number" used for the high-symmetry structures.

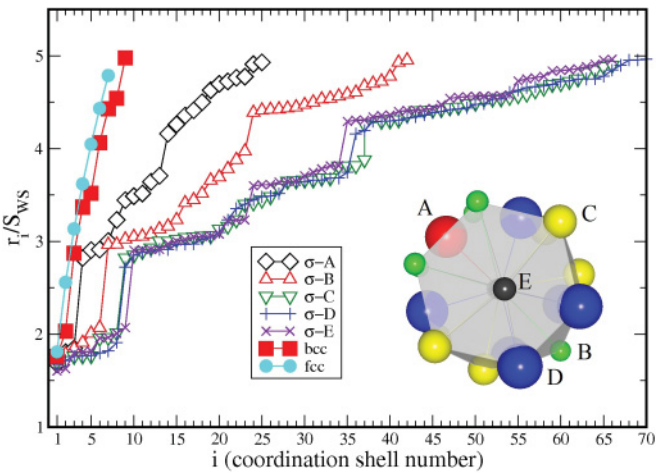

FIG. 2. (Color online) Radii of coordination shells (in units of the Wigner-Seitz radii of the corresponding structures) of the five sublattices of the σ phase (*A*,*B*,*C*,*D*,*E*), bcc and fcc structures versus the coordination shell number.

TABLE I. Effective pair interactions (ECIs) (in mRy) in the σ phase within the range of polyhedra of the closest sites; n_i^{cs} is the coordination number (number of sites at the ith coordination shell) with a radius r_i (in units of the Wigner-Seitz radius S_{WS}). For the first composition the one-electron contribution $V_i^{(2)-\mathrm{one}-el}$ is specified in addition to the total GPM interaction $V_i^{(2)-tot}$.

Subl. type	Coord. shell	n_i^{cs}	r_i/S_{WS}	$Fe_{0.5}Cr_{0.5}$ $V_i^{(2)-\mathrm{one}-el}$	$Fe_{0.5}Cr_{0.5}$ $V_i^{(2)-tot}$	$Fe_{0.4}Cr_{0.6}$ $V_i^{(2)-tot}$
A-D	1	4	1.6770	2.319	4.730	4.495
A-E	2	4	1.8051	0.914	2.931	2.567
A-B	3	4	1.8465	0.009	1.846	1.450
B-C	1	2	1.7160	−2.103	−0.362	0.000
B-B	2	1	1.7878	0.985	2.506	2.601
B-A	3	2	1.8465	0.009	1.846	1.450
B-D	4	4	1.9094	−0.959	0.372	0.028
B-E	5	4	2.0091	−1.184	−0.121	−0.294
B-E	6	2	2.0715	−1.323	−0.564	−0.597
C-C	1	1	1.6987	−2.819	−0.991	−0.473
C-B	2	1	1.7160	−2.103	−0.362	0.000
C-D	3	2	1.7604	1.643	3.739	3.652
C-D	4	1	1.7646	0.434	2.529	2.574
C-D	5	1	1.7675	0.394	2.489	2.569
C-E	6	2	1.9578	−0.481	0.634	0.556
C-E	7	2	1.9640	−0.906	0.210	0.132
C-C	8	4	2.0133	−1.319	−0.405	−0.753
D-A	1	1	1.6770	2.319	4.730	4.495
D-D	2	1	1.7160	2.856	5.258	5.147
D-C	3	2	1.7604	1.643	3.739	3.652
D-C	4	1	1.7646	0.434	2.529	2.574
D-C	5	1	1.7675	0.394	2.489	2.569
D-E	6	2	1.7949	0.478	2.299	2.284
D-E	7	2	1.8183	0.598	2.242	2.239
D-B	8	2	1.9094	−0.959	0.372	0.028
E-E	1	1	1.6026	0.191	2.358	4.511
E-E	2	1	1.6287	−1.076	1.091	2.708
E-D	3	2	1.7949	0.478	2.299	2.284
E-A	4	1	1.8051	0.914	2.931	2.567
E-D	5	2	1.8183	0.598	2.242	2.239
E-C	6	2	1.9578	−0.481	0.634	0.556
E-C	7	2	1.9640	−0.906	0.210	0.132
E-B	8	2	2.0091	−1.184	−0.121	−0.294
E-B	9	1	2.0715	−1.323	−0.564	−0.597

In Fig. 2 we plot the coordination shell radii (in units of the corresponding Wigner-Seitz radius S_{WS}) for the five sublattices of the σ phase in comparison to those for the bcc and fcc structures within approximately the same distance up to $r_i/S_{WS} = 5$, which is equivalent to the range of seven and nine coordination shells for the fcc and bcc structures, respectively. The number of sites within this distance is approximately the same (about 130) independent of the structure and the sublattice type of the σ phase. However, one can clearly see the huge difference in the number of coordination shells (within this range) between the simple Bravais lattices and the different sublattices of the σ phase, in particular, the huge number of coordination shells for sublattices C, D, and E, close to 70. This clearly means that these coordination shells consist, on average, of less than just two sites. The structural isolation of the σ-phase sites results in a kind of gap for the relative radii of the coordination shells between 2.1 and 2.8, which can be seen in Fig. 2. In other words, the coordination numbers are the number of sites within a range of relative distances up to about $r/S_{WS} = 2.1$. Such a gap can also be seen between the second and third coordination shells of the bcc structure (see Fig. 2) and to some extent between the radii of the first and second coordination shells of the fcc lattice.

The coordination number within this range for the bcc structure is 14 (the first two coordination shells) and 12 (just the first coordination shell) for the fcc structure. On the basis of such consideration, one may say that the A and D sublattices have the nearest-neighbor environment closer to that of the fcc structure (coordination number 12), while other sublattices have an environment which is closer to that of the bcc structure. This appears to be important for the site substitution behavior, since as has been mentioned above, the A and D sublattices are mostly occupied by the Fe atoms.

The information presented in Fig. 2 serves the purpose of demonstrating the problem related to extracting the ECI using a structure inversion method. The number of different effective pair interactions $V_i^{(2)}$ just within a polyhedron of the closest sites (or within the relative range of the first two coordination shells of the bcc structure) is 20 (see Table II: note that interactions between different sites are listed there twice), while the number of inequivalent multisite interactions is much larger, even within such short distances. In fact, this makes the structure inversion method for the Hamiltonian (1) impractical for the σ phase.

B. Effective cluster interactions

The ECI parameters can be directly calculated by the generalized perturbation method (GPM).[21–23] The screening contribution,[24] which is needed for the calculation of the effective pair interactions, is quite difficult to obtain because of the huge size of the supercell that would be needed to model a random alloy with the σ-phase structure. Therefore, we assume that the screened Coulomb interaction contribution is similar to that in the bcc structure and depends linearly on the distance within the range of the first two coordination shells. This is, of course, an approximation, but one that is justified for the main purpose of our calculations in this section, namely, to check the qualitative picture of the effective interactions in the σ phase.

In Fig. 3 we first show the one-electron contribution to the screened GPM effective pair interactions calculated up to $r_i/S_{WS} = 5$ for the $Fe_{0.5}Cr_{0.5}$ system. These interactions were obtained by the screened GPM method (SGPM) on the basis of local density approximation (LDA) self-consistent calculations of the electronic structure for these alloys for which the paramagnetic disordered local moment (DLM)[25] state was assumed for the Fe species. The calculations were done for a high-temperature lattice parameter of the σ phase by applying the exact muffin-tin orbital (EMTO) method[26] within the coherent potential approximation (CPA),[27] where the Fermi function smearing (corresponding to a temperature of 1100 K) was used. One can see that the effective interactions decay very fast with distance, where the strongest interactions are those at short distances.

More details about effective interactions within the range of the polyhedra of the closest sites are given in Table I,

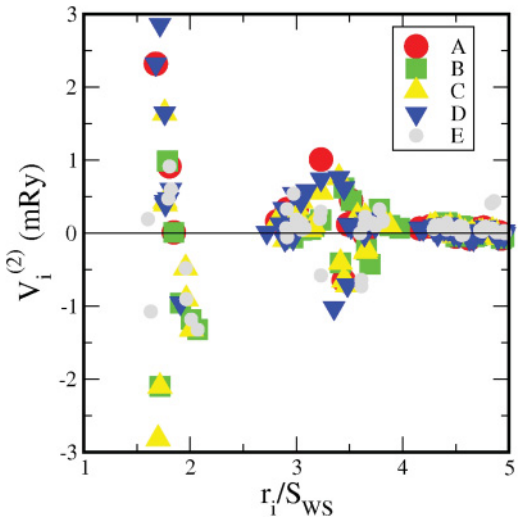

FIG. 3. (Color online) One-electron contribution to the effective pair interactions obtained by the generalized perturbation method (GPM).

where we present the effective pair interactions for two alloy compositions, namely, $Fe_{0.5}Cr_{0.5}$ and $Fe_{0.4}Cr_{0.6}$. For the first composition we also specify the one-electron contribution (without the screened Coulomb interaction) to the total GPM interaction. It is clear that the screening contribution is about 1–2 mRy and thus is of the same order as the other term and makes the total GPM interactions more positive, that is, of ordering type. However, the SGPM yields only chemical effective interactions, i.e., the interactions on a fixed ideal underlying lattice. Although the size mismatch between Fe and Cr is relatively small, one still can expect contributions from strain-induced interactions, which originate from local lattice relaxations due to a change in the alloy configuration. In the case of bcc Fe-Cr alloys, the contribution of the strain-induced interactions at the first coordination shell is about -1.0 to -1.5 mRy.[28] This means that it partly compensates the contribution from the screened Coulomb interactions.

The main conclusion from the results presented above is that the strongest nearest-neighbor effective interactions in the FeCr σ phase are of an ordering type and have values of 0–3 mRy. This means that they are weak and cannot produce substantial ordering effects above 800 K, neither on the same sublattice nor between different sublattices, especially when taking into account the fact that the coordination numbers are small. As one can see, there is a certain concentration dependence of the effective pair interactions, but in most cases it is quite weak, except for the first two coordination shells of the sublattice E. However, these coordination shells consist of only one site and thus their contribution to the average concentration dependence of the effective interactions is negligible.

We have also calculated some of the three- and four-site ECIs within the polyhedron of the closest sites, but most of them are less than 0.1 mRy. The strongest three-site interaction, 0.7 mRy, is for the triangle formed by one B site and two A sites, which correspond to the second and third coordination shells of the B sublattice (see Table I). The strongest four-site interaction, -0.48 mRy, is for a tetrahedron formed by two A and two B sites. Two B sites and each A site form the triangle described above, while the A sites are at the eighth coordination shell relative to each other. It is clear that such interactions cannot produce a large effect on the ordering energetics at the temperatures of interest. Besides, the contribution from three-site interactions on the ordering energy is practically negligible, at least close to the equiatomic composition.

With the analysis given above we can assume that (1) the free energy of the σ phase can be quite accurately presented in terms of *concentration-independent* cluster interactions, (2) the dominating terms in this expansion are the on-site interactions $V_i^{(1)}$, as shown below, and finally (3) the single-site mean-field approximation will be sufficient to provide a reasonably accurate description of the configurational effects at high temperatures.

III. SINGLE-SITE MODEL FOR THE FREE ENERGY

At high temperature, where atomic short-range order effects are relatively weak, we assume that the Helmholtz free energy F for a given composition $c \equiv c_{Cr}$ and temperature T is

$$F(\{c_\alpha\}) = E_{\text{tot}}(\{c_\alpha\}) - T(S_{\text{conf}} + S_{\text{magn}}). \tag{2}$$

Here $E_{\text{tot}}(\{c_\alpha\})$ is the total energy of the $Fe_{1-x}Cr_x\sigma$ phase, whose sublattices are completely random and have the corresponding site occupations $\{c_\alpha\}$, where c_α is the concentration of Cr in site (sublattice) α ($\alpha = A,B,C,D,E$).

For a fixed composition the total energy (per unit cell) $E_{\text{tot}}(\{c_\alpha\})$ can be written in a simplified form as

$$E_{\text{tot}}(\{c_\alpha\}) = E_0(c) + \sum_{\alpha=1,4(A,D)} n_\alpha J_\alpha^{(1)} c_\alpha + \frac{1}{2} \sum_{\alpha,\beta=1,4(A,D)} n_\alpha n_\beta J_{\alpha\beta}^{(2)} c_\alpha c_\beta, \tag{3}$$

where n_α is the number of sites at sublattice α.

Here the summation runs only over four sublattices, since the concentration at the fifth sublattice is determined from the alloy concentration c and the concentrations at the other four sublattices c_α. $E_0(c)$ is the total energy of a homogeneous random alloy ($c_\alpha = c$), and $J_\alpha^{(1)}$ and $J_{\alpha\beta}^{(2)}$ are the on-site and pair (or second-order) interaction parameters.

The on-site interaction parameter $J_\alpha^{(1)}$ is the zero-temperature relative effective chemical potential which can be determined as

$$J_\alpha^{(1)} = [\partial E_{\text{tot}}/\partial c_\alpha - \partial E_{\text{tot}}/\partial c_E]|_{c_{\text{alloy}}=c} \tag{4}$$

and describes the preference of Cr atoms to occupy site α relative to that of sublattice E. If there is no dependence on $\{c_\alpha\}$ of the ECI in (1), $J_\alpha^{(1)} = V_\alpha^{(1)} - V_{\alpha=E}^{(1)}$.

The second-order interaction parameters are determined in a similar way:

$$J_{\alpha\beta}^{(2)} = [\partial^2 E_{\text{tot}}/(\partial c_\alpha \partial c_\beta) - \partial^2 E_{\text{tot}}/(\partial c_\alpha \partial c_E) - \partial^2 E_{\text{tot}}/(\partial c_\beta \partial c_E) + \partial^2 E_{\text{tot}}/(\partial c_E \partial c_E)]|_{c_{\text{alloy}}=c}. \tag{5}$$

As in the case of the on-site parameters $J_{\alpha}^{(1)}$ they can also be expressed through effective pair interactions of the Hamiltonian defined in Eq. (1):

$$J_{\alpha\beta}^{(2)} = \sum_{j\in\beta} V_{\alpha\beta;0j}^{(2)} - \sum_{j\in E} V_{\alpha E;0j}^{(2)} - \sum_{j\in\beta} V_{\beta E;0j}^{(2)} + \sum_{j\in E} V_{EE;0j}^{(2)}, \tag{6}$$

that is, $J_{\alpha\beta}^{(2)}$ presents an "integral" information about effective pair interactions.

Temperature effects are described by the second term in Eq. (2), which takes the configurational and magnetic entropy into account. We neglect contributions from lattice vibrations, assuming that they do not play a decisive role in the distribution of the components between the sublattices. Since the relevant temperatures are relatively high and there is no experimental evidence of being close to any kind of phase transition (ordering or magnetic), we also neglect contributions from short-range order effects in the configurational part of the problem. The configurational entropy (per unit cell) in Eq. (2) is then defined as

$$S_{\text{conf}} = -k_B \sum_{\alpha=1,5} n_{\alpha} \left[c_{\alpha} \ln c_{\alpha} + (1-c_{\alpha}) \ln(1-c_{\alpha})\right]. \tag{7}$$

The importance of magnetism in the Fe-Cr σ phase, even at the relevant high temperatures, was recognized by Korzhavyi *et al.*,[13] who considered a spin-polarized paramagnetic state of this phase as described by the DLM model. In this work it has been shown that even at these temperatures the local magnetic moments do not disappear on the Fe atoms (but vanish for the Cr atoms) but make an important contribution to the energetics of the σ phase.

As already discussed in our previous work,[19] the Fe-Cr σ phase is a weak itinerant magnet and thus another magnetic contribution should also appear at high temperatures, namely, longitudinal spin fluctuations, which are thermal Stoner-like many-body excitations that lead to fluctuations of the magnitude of the local magnetic moments of Fe and Cr. To calculate these high-temperature magnetic excitations by accurate first-principles schemes would be extremely computationally demanding. Therefore we adopt a simple model[29] which implies that longitudinal spin fluctuations (LSFs) contribute to the magnetic entropy of the paramagnetic state.

In particular, LSFs induce modified spin magnetic moments on Fe and Cr atoms, while the Cr atoms would have zero magnetic moments in the DLM state. The corresponding magnetic entropy in Eq. (2) is given by the following expression:

$$S_{\text{magn}} = k_B \sum_{\alpha=1,5} n_{\alpha} \left[c_{\alpha} \ln\left(1+\mu_{\alpha}^{Cr}\right) + (1-c_{\alpha}) \ln\left(1+\mu_{\alpha}^{Fe}\right)\right], \tag{8}$$

where the local magnetic moments are found by minimizing the corresponding magnetic free energy in the first-principles calculations at a given temperature.

IV. FIRST-PRINCIPLES CALCULATIONS

The energy derivatives of the total energies have been evaluated for the random alloys close to the equiatomic composition by the exact muffin-tin orbital (EMTO) method within the full charge density formalism (FCD).[30] The EMTO method is an improved screened Korringa-Kohn-Rostoker method, where large overlapping potential spheres are used for accurately describing the exact single-electron potential. The FCD method was devised to perform with high efficiency as well as with an accuracy of full potential total energy methods.[26] For the exchange-correlation functional the generalized gradient approximation was taken.[31]

In the present work we use the CPA[27] to determine the electronic structure of random alloys on sublattices of the σ phase. The coefficient for screened Coulomb interactions have been chosen to be $\alpha_{scr} = 0.67$ and $\beta_{scr} = 1.05$ for all the sublattices. Obviously this is an approximation, but supercell calculations of the screening constants would be impractical for many reasons. For instance, it would be impossible to calculate the electronic structure of a reasonably small supercell (up to several thousand atoms) such that all the atomic short-range order parameters would be as in a perfectly random alloy (at least within the range of interactions as presented in Table I). Another approximation in the present work is that local atomic relaxations have been ignored. As has been demonstrated in Ref. 19, their effect on the formation enthalpy is not greater than 0.1 kJ/mol.[19] The latter is due to the similar atomic sizes of Fe and Cr.

A. CPA-LSGF

The applicability of the CPA to the electronic structure calculations of random alloys, and in particular the case of the Fe-Cr σ phase, can be checked using methods going beyond the single-site approximation. The best choice in this particular case is the locally self-consistent Green's function technique,[32] implemented within the EMTO method (LSGF-EMTO).[33] This method allows one to calculate the electronic structure of large supercells modeling random alloys that are built upon the corresponding underlying lattice. The latter determines the symmetry and structure of the effective medium, which is obtained using the CPA for all the atoms on the sublattices in the supercell. The effective medium provides the boundary condition for a local interaction zone consisting of a given atom and several coordination shells in the Green's function calculations of the electronic structure of this atom. Solving such a (Dyson) equation for every atom in the supercell produces the electronic structure of the whole supercell.

The supercell representing a random alloy is usually chosen to have certain atomic distribution correlation functions which are the same as they would be in a real random alloy. However, the problem in the case of the σ phase is that quite a large number of correlation functions should be optimized, even if only the pair correlation functions of the polyhedra of the closest sites are considered. Therefore we have used a simplified procedure that can work quite reasonably for large supercells. Namely, we have randomly distributed atoms in a $4 \times 4 \times 4(\times 30)$ supercell (1920 atoms in total) using only the condition that the number of Cr and Fe atoms should

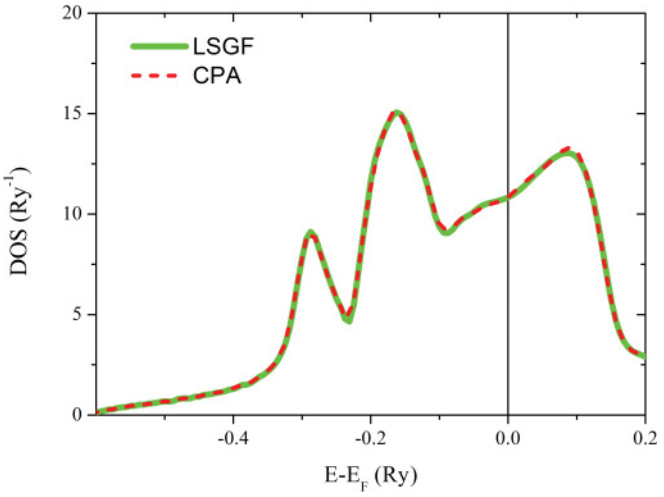

FIG. 4. (Color online) Total density of states (DOSs) of the $Fe_{0.5}Cr_{0.5}$ σ phase obtained in the LSGF supercell and CPA calculations.

be the same at each sublattice. This is the way we represent the $Fe_{0.5}Cr_{0.5}$ random alloy. Two supercells, SC1 and SC2, have been constructed in this way for the LSGF electronic structure calculations.

The LSGF-EMTO calculations have been done using the same setup of parameters as in the usual EMTO-CPA calculations in the DLM state. The local interaction zone included the polyhedron of the nearest neighbors for each site. In Fig. 4 we show the density of states for the $Fe_{0.5}Cr_{0.5}$ σ phase obtained in the supercell LSGF and CPA calculations. They are practically indistinguishable, which means that the CPA is quite accurate for this system. This is so in spite of the fact that there exist very strong fluctuations of the local magnetic moments of Fe atoms in the σ phase.

In Fig. 5 we show the local magnetic moments of the Fe atoms on the different sublattices in one of the calculated supercells, the average magnetic moments of Fe on the

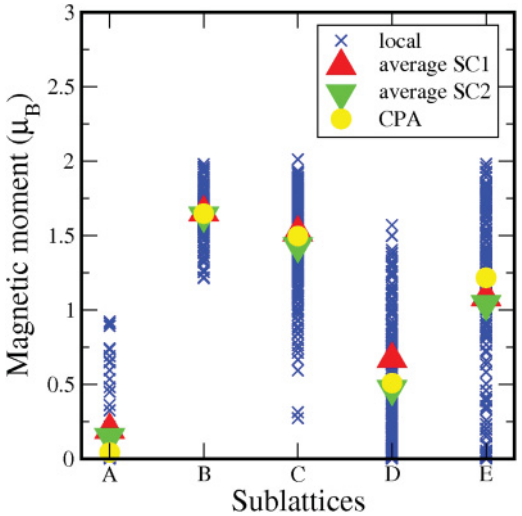

FIG. 5. (Color online) Local magnetic moments of Fe in the supercells in the LSGF calculation, average magnitudes in two supercells (SC1 and SC2), and the CPA result.

sublattices in both supercells, and the corresponding CPA result. There is a huge dispersion of the magnetic moments, especially on the sublattices C, D, and E in the supercell. Nevertheless, the average magnetic moments of the supercells agree quite well with each other. It is also clear that the CPA results are in very good agreement with those of the LSGF calculations for supercells.

V. RESULTS AND DISCUSSION

A. Convergence of the total energy parametrization

As described in Sec. III, the single-site model implies the expansion of the total energy in terms of effective interactions, which we determine as the derivatives of the total energy with respect to the sublattice occupancies [see Eq. (3)]. In general, these interactions could be calculated using the usual least-squares-fit method of the total energies, but this requires much more computational effort, especially taking into account that they are temperature dependent (see below). Since we want also to study how the atomic distribution depends on different magnetic states and structural variations, we would like to stay within the single-site model and use only the on-site effective interactions determined by Eq. (4).

However, in order to check the accuracy of the on-site form of the energy expansion, we calculate the total energies of 89 different σ-phase configurations for $x_{Cr} = 0.50$ in the DLM state with different sublattice occupancies and obtain parameters of the total energy expansion up to the second order using the least-mean-squares method. The calculated parameters $\tilde{J}^{(1)}_{\alpha}$,$\tilde{J}^{(2)}_{\alpha\beta}$ are given in Table II. First, one can see that the pair interaction parameters are much weaker than the on-site ones and therefore their contribution to the total energy would be rather small. At the same time, the on-site interactions obtained using Eq. (4) are very close to the corresponding least-squares values $\tilde{J}^{(1)}_{\alpha}$. This means that the dependency of the energy on the site occupancies is quite smooth and therefore we can stay within the on-site approach, keeping only contributions from chemical potentials to the total energy.

B. Effect of the magnetic state

In this section we analyze how magnetism affects the site distribution of Fe and Cr atoms in the σ phase. For this purpose

TABLE II. Effective cluster interactions (ECIs) calculated for the experimental lattice volume $V_{\text{exp}} = 0.35271$ nm^3 and $(c/a)_{\text{exp}} = 0.518$ at $T = 1000$ K in the DLM state once as chemical potentials $J^{(1)}_{\alpha}$ [according to Eq. (4)] and once using a least-squares fit ($\tilde{J}^{(1)}_{\alpha}$,$\tilde{J}^{(2)}_{\alpha\beta}$) in mRy/cell.

ECI	A	B	C	D	E
$\tilde{J}^{(1)}_{\alpha}$	16.095	0.867	1.480	15.415	0
$J^{(1)}_{\alpha}$	16.406	0.469	1.781	14.344	0
$\tilde{J}^{(2)}_{\alpha\beta}$	A	B	C	D	E
A	−1.198	−0.371	−0.648	−0.457	0
B		−0.490	−0.390	−0.463	0
C			−0.568	−0.407	0
D				−0.640	0
E					0

TABLE III. Effective on-site interactions $J_\alpha^{(1)}$ (mRy/cell) calculated for the experimental lattice volume $V_{\rm exp} = 0.35271$ nm^3 and $(c/a)_{\rm exp} = 0.518$ at $T = 1000$ K in different magnetic states.

Site	NM	DLM	DLM with LSF
A	19.031	16.406	15.750
B	−0.656	0.469	0.281
C	2.344	1.781	1.969
D	15.750	14.344	13.406
E	0.0	0.0	0.0

we calculate the site occupancies as a function of temperature in three different magnetic states: (i) the nonmagnetic state (NM), in which the effect of spin polarization is completely neglected, (ii) the paramagnetic state given by the usual DLM model, and (iii) the paramagnetic state (again given by the DLM model) but including the longitudinal spin fluctuations (LSFs). The latter are many-body Stoner excitations, which can in an approximate way be included in the usual DFT scheme by assuming that they lead to an additional contribution to the entropy given by Eq. (8), a situation for which the magnetic moment can be determined from a Helmholtz free energy minimization.

The corresponding on-site parameters $J_\alpha^{(1)}$ calculated for the experimental lattice volume $V_{\rm exp} = 0.35271$ nm^3 and $(c/a)_{\rm exp} = 0.518$ at $T = 1000$ K are given in Table III. One can see that the difference between interaction parameters in different magnetic states is rather small, especially in the case of the DLM interactions with and without LSFs. Nevertheless, the magnetism produces a substantial effect on the site substitution behavior in the high-temperature range, which is, of course, mostly an entropy effect.

In Fig. 6 we show the results of the minimization of the free energy given in Eq. (2) with the total energy from Eq. (3) obtained for the on-site interaction parameters given in Table III. The full symbols denote the calculated site occupancies, while the empty symbols show the available experimental data,[2,4] and the vertical lines indicate the narrow temperature range of the σ-phase formation, $700 < T < 1100$ K. As can be seen, the configurational entropy drives the system at very high temperatures to a highly disordered distribution of alloy components on the five nonequivalent sites. When the temperature is decreased, Fe and Cr atoms exhibit a preference for different sites. At temperatures of about 700 K, which is the lower border of the σ-phase stability range, the (*A*,*D*) sites become solely occupied by Fe atoms (i.e., nearly no Cr atoms), the (*B*,*E*) sites mostly by Cr atoms, while the occupation of C sites remains almost the same. This is a common behavior that is independent of the magnetic state.

Nevertheless, there are important differences when looking at the details. For instance, neglecting the magnetic entropy causes an underestimation of the Cr concentration on the *A* and *D* sublattices, while the *B* and *E* sublattices have an excess of Cr atoms in comparison with the DLM results (without the LSF), as well as the experimental data. Therefore it is clear that the magnetic entropy has a noticeable effect on the site preference of Fe and Cr atoms. One can also see that the inclusion of the longitudinal spin fluctuations affects the site occupation of the B sites and increases the content of Cr. Let us note that our theoretical results presented in Fig. 6 are in good agreement with experimental data. There can be many reasons for small discrepancies, from which we analyze the structural effects in the next section.

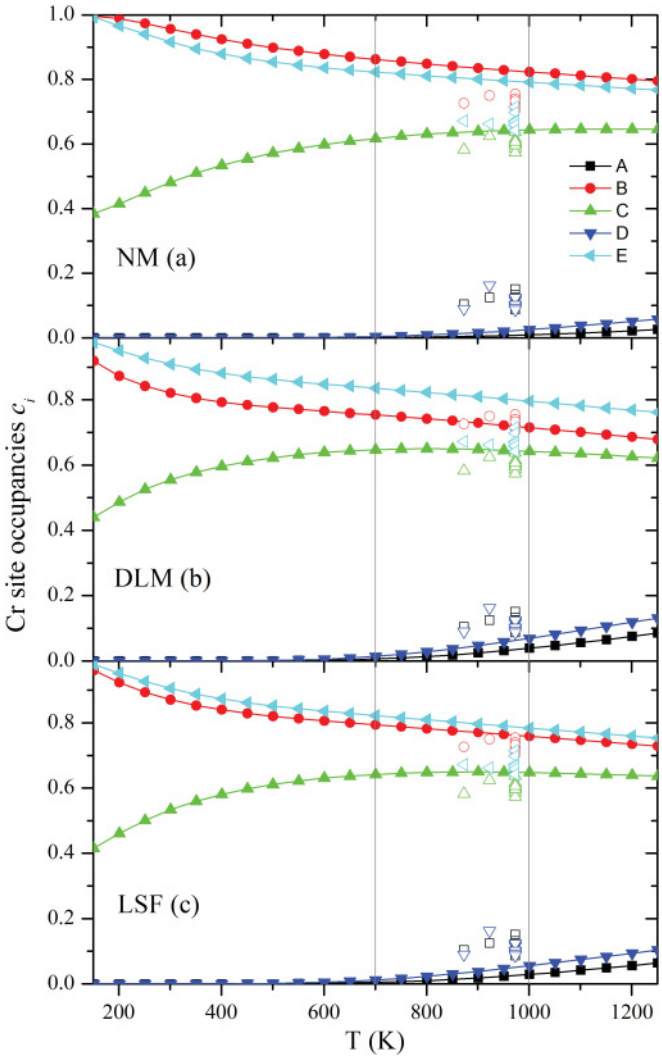

FIG. 6. (Color online) The Cr site occupancies of the (*A*,*B*,*C*,*D*,*E*) sublattices versus temperature for $x_{Cr} = 0.50$ calculated for the experimental lattice parameters $V_{\rm exp} = 0.35271$ nm^3 and $(c/a)_{\rm exp} = 0.518$ in different magnetic states: (a) nonmagnetic state (NM), (b) disordered local moment state (DLM), (c) disordered local moment state including longitudinal spin fluctuations (LSFs). The full symbols denote the calculated results, and the empty symbols the available experimental data.[2,4] The vertical lines indicate the temperature range of the σ-phase formation in the Fe-Cr alloy.

C. Structural variations

In order to study the effect of structural variations (volume and also the c/a ratio) we calculate the site occupancies for four different sets of parameters (a–d) given in Table IV. The change of volume at constant $c/a = 0.518$ from the experimental low-temperature value $V_{\rm exp} = 0.35271$ nm^3 [set (a)] to the high-temperature value $V = 0.36247$ nm^3 [set (b)] increases the Cr occupancy for the (*A*,*D*) sites while decreasing

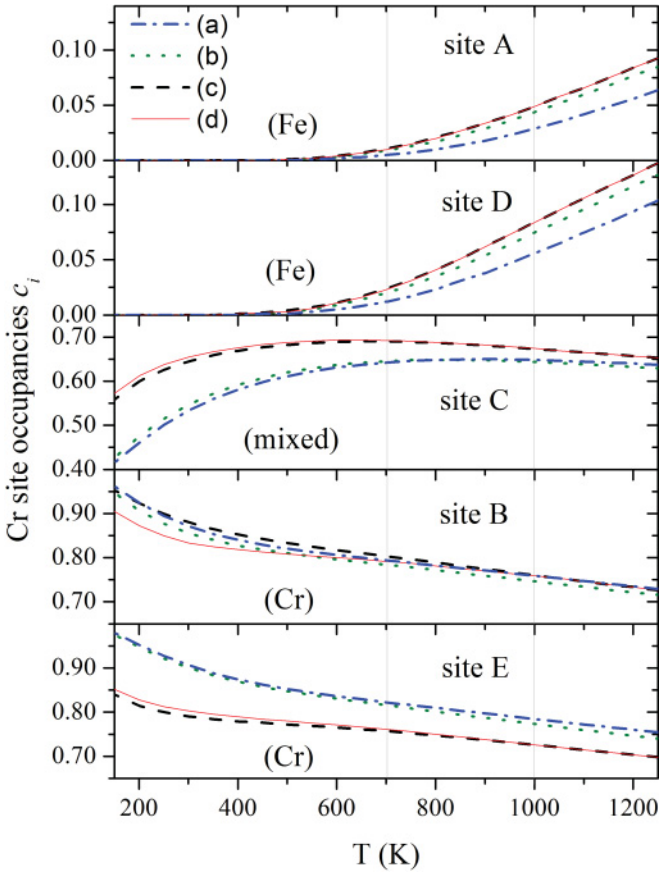

FIG. 7. (Color online) The Cr site occupancies of the (*A*,*B*,*C*,*D*,*E*) sublattices for four different sets of structural parameters given in Table IV. In parenthesis we specify the element which predominately occupies the given sublattice $\alpha = (A,B,C,D,E)$.

the Cr content in the (*B*,*E*) sites (see Fig. 7). The volume expansion [from set (a) to set (b)] increases the available space (see Fig. 1) around the (*A*,*D*) sublattices and thus favors occupation by the bigger Cr atoms. We have also optimized the c/a ratio using the EMTO-CPA method for the high-temperature volume [set (c) in Table IV]. It can be clearly seen from Fig. 7 [sets (b) and (c)] that although c/a changes only very little, it produces a remarkable decrease of the Cr occupancy of the E site with a corresponding increase at the other sites, mainly the *C* site. With the c/a expansion the average volume of the *E* sublattice decreases, while it increases for the *C* sublattice. At the same time the occupation of the 12-coordinated *A* and *D* sites by large Cr atoms is not favored, since this would lead (within the kagome layers of the σ phase) to a distortion that would act against the structural stability.[34]

TABLE IV. Structural variation and temperature dependency for the $Fe_{0.5}Cr_{0.5}$ σ phase in the DLM state including LSF.

Set	Volume	c/a	*T* dependency
a	0.35271 nm^3	0.5180	No
b	0.36247 nm^3	0.5180	No
c	0.36247 nm^3	0.5232	No
d	0.36247 nm^3	0.5232	Yes

TABLE V. On-site parameters $J_\alpha^{(1)}$ (mRy/cell) and local magnetic moments of Fe and Cr atom μ_α^{Fe} and μ_α^{Cr} calculated for expanded lattice parameters $V = 0.36247$ nm^3 and $c/a = 0.5232$ at $T = 500$, 1000 K (DLM incl. LSF).

	T (K)	*A*	*B*	*C*	*D*	*E*
$J_\alpha^{(1)}$ (mRy/cell)	500	13.219	−0.375	0.656	11.250	0.0
	1000	12.937	−0.656	0.656	10.969	0.0
$\mu_\alpha^{Fe}(\mu_B)$	500	0.847	1.742	1.585	1.074	1.404
	1000	1.046	1.773	1.626	1.236	1.478
$\mu_\alpha^{Cr}(\mu_B)$	500	0.171	0.286	0.245	0.198	0.203
	1000	0.306	0.481	0.380	0.350	0.358

D. Temperature effects

Furthermore, the use of the DLM model including LSFs implies that the local magnetic moments of Fe and Cr at different sublattices $\mu_\alpha^{Fe(Cr)}$ depend on temperature making the interaction parameters $J_\alpha^{(1)}$ temperature dependent. In Table V we list the values of $J_\alpha^{(1)}$ and $\mu_\alpha^{Fe(Cr)}$ calculated at 500 and 1000 K. One can notice that in general the temperature dependence of the on-site interaction parameters $J_\alpha^{(1)}$ is very small and is visible only for the B site, which is mostly occupied by Cr. In common DLM calculations μ_α^{Cr} is zero at those temperatures, but the LSFs produce a finite Cr moment with a fairly pronounced *T* dependency. It should be mentioned here that an increase of local magnetic moments is possible in a simple LSF model used in the present work[29] and is due to the entropic effect. As can be seen from Fig. 7 [set (d)] temperature dependence of $\mu_\alpha^{Fe(Cr)}$ and $J_\alpha^{(1)}$ causes a decrease of the Cr site occupation of the B site, but this is evident only at low temperatures, whereas almost no effect can be seen at high temperatures.

E. Final results and summary

In order to get the proper atomic distribution which takes into account all effects described above (magnetic state, struc-

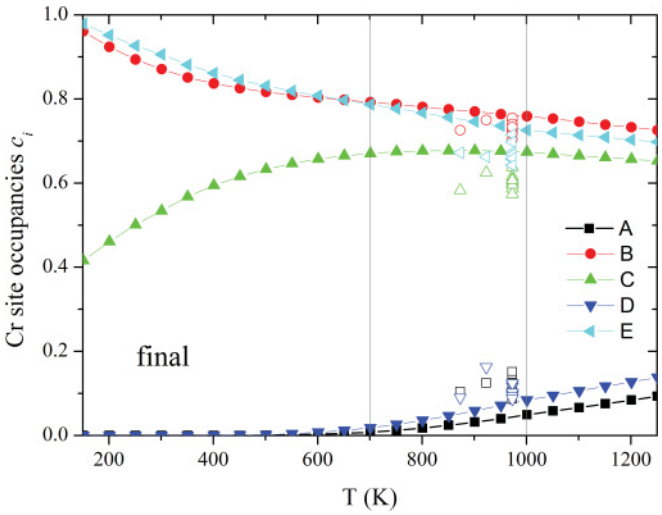

FIG. 8. (Color online) The Cr site occupancies of the (*A*,*B*,*C*,*D*,*E*) sublattices versus temperature including all effects mentioned. The empty symbols denote the available experimental data.[2,4]

tural variations, and temperature effects), we interpolate the Cr site occupancies between the low- and high-temperature values that were obtained for the experimental room-temperature lattice parameters and temperature-expanded ones. The results are shown in Fig. 8 and agree quite well with the available experimental data.[2,4] It is interesting to note that the preference of the Cr atoms between the B and E sites crosses at around 650–700 K, at a temperature where the σ-phase formation starts. The occupation behavior for other sites also changes at this temperature, as discussed above.

In the present work we studied the configurational thermodynamics of the Fe-Cr σ phase on the basis of the Ising-type configurational Hamiltonian and a single-site mean-field model for the free energy. The effective pair interactions in the σ phase are relatively small and thus the mean-field model can be used in a simplified form in which only contributions from effective on-site interactions are included.

Using this model we demonstrate that the site occupation behavior is governed by several factors. The magnetic entropy contributes mainly to the (A,D) and B sites, whereas the structural variations (volume and c/a), which might be present in the system due to effects of the neutron irradiation and thermal expansion, lead to an additional atomic redistribution. In particular, the volume expansion allows to accumulate more Cr in the A and D sublattices, while the c/a ratio affects the occupation of the C sites.

ACKNOWLEDGMENTS

This work was partly supported by the Austrian Science Fund (FWF) within the Science College CMS (Grant W004) and the special research program ViCoM (Grant F41). A.V.R. and B.J. are grateful to the Swedish Research Council (VR) and Hero-m Centrum, Jernkontoret, and ERC grant for financial support.

[1] J. L. Garin and R. L. Mannheim, J. Mater. Process. Technol. **209**, 3143 (2009).
[2] H. L. Yakel, Acta Crystallogr. Sect. B **39**, 20 (1983).
[3] J. Cieślak, M. Reissner, W. Steiner, and S. Dubiel, J. Magn. Magn. Mater. **310**, e613 (2007).
[4] J. Cieślak, M. Reissner, S. Dubiel, J. Wernisch, and W. Steiner, J. Alloys Compd. **460**, 20 (2008).
[5] D. Read and E. Thomas, J. Phys. Chem. Solids **29**, 1569 (1968).
[6] Y. Sumitomo, T. Moriya, I. Hiromitsu, and F. Fijita, J. Phys. Soc. Jpn. **35**, 461 (1973).
[7] J. Cieślak, B. Costa, S. Dubiel, M. Reissner, and W. Steiner, J. Phys.: Condens. Matter **17**, 2985 (2005).
[8] J. Cieślak, M. Reissner, W. Steiner, and S. Dubiel, Phys. Stat. Sol. (a) **8**, 1794 (2008).
[9] F. C. Frank and J. S. Kasper, Acta Crystallogr. **11**, 184(1958).
[10] J. S. Kasper and R. Waterstrat, Acta Crystallogr. **9**, 289 (1956).
[11] M. H. F. Sluiter, K. Esfarjani, and Y. Kawazoe, Phys. Rev. Lett. **75**, 3142 (1995).
[12] J. Havránková, J. Vrešťál, L. G. Wang, and M. Sob, Phys. Rev. B **63**, 174104 (2001).
[13] P. Korzhavyi, B. Sundman, M. Selleby, and B. Johansson, Mater. Res. Soc. Symp. Proc. **842**, S4.10 (2005).
[14] E. Kabliman, A. Mirzoev, and A. Udovskii, Phys. Met. Metallogr. **108**, 435 (2009).
[15] J. Pavlu, J. Vřešťál, and M. Šob, Intermetallics **18**, 212 (2010).
[16] J. Cieślak, J. Tobola, and S. M. Dubiel, e-print arXiv:1103.4260v1 [cond-mat.mtrl-sci] (2011).
[17] J. W. D. Connolly and A. R. Williams, Phys. Rev. B **27**, 5169 (1983).
[18] M. Palumbo, T. Abe, S. G. Fries, and A. Pasturel, Phys. Rev. B **83**, 144109 (2011).
[19] E. Kabliman, P. Blaha, K. Schwarz, A. V. Ruban, and B. Johansson, Phys. Rev. B **83**, 092201 (2011).
[20] E. Kabliman, A. V. Ruban, P. Blaha, and K. Schwarz, Solid State Phenom. **170**, 13 (2011).
[21] F. Ducastelle and F. Gautier, J. Phys. F **6**, 2039 (1976).
[22] F. Ducastelle, *Order and Phase Stability in Alloys* (North-Holland, Amsterdam, 1991).
[23] A. V. Ruban, S. Shallcross, S. I. Simak, and H. L. Skriver, Phys. Rev. B **70**, 125115 (2004).
[24] A. V. Ruban and H. L. Skriver, Phys. Rev. B **66**, 024201 (2002); A. V. Ruban, S. I. Simak, P. A. Korzhavyi, and H. L. Skriver, *ibid.* **66**, 024202 (2002).
[25] B. L. Gyorffy, A. J. Pindor, J. Staunton, G. M. Stocks, and H. Winter, J. Phys. F **15**, 1337 (1985).
[26] L. Vitos, *Computational Quantum Mechanics for Materials Engineers: The EMTO Method and Applications* (Springer, London, 2007).
[27] B. Györffy, Phys. Rev. B **5**, 2382 (1972).
[28] M. S. Blanter, Phys. Status Solidi B **181**, 377 (1994).
[29] V. Heine and R. Joynt, Europhys. Lett. **5**, 81 (1988).
[30] L. Vitos, Phys. Rev. B **64**, 014107 (2001); L. Vitos, I. A. Abrikosov, and B. Johansson, Phys. Rev. Lett. **87**, 156401 (2001).
[31] J. P. Perdew, K. Burke, and M. Ernzerhof, Phys. Rev. Lett. **77**, 3865 (1996).
[32] I. A. Abrikosov, A. M. N. Niklasson, S. I. Simak, B. Johansson, A. V. Ruban, and H. L. Skriver, Phys. Rev. Lett. **76**, 4203 (1996); I. A. Abrikosov, S. I. Simak, B. Johansson, A. V. Ruban, and H. L. Skriver, Phys. Rev. B **56**, 9319 (1997).
[33] O. E. Peil, A. V. Ruban, and B. Johansson (in preparation).
[34] F. J. Spooner, Acta Crystallogr. Sect. A **24**, 605(1968).